Aligned-Braided Nanofibrillar Scaffold with Endothelial Cells Enhances Arteriogenesis

Karina H. Nakayama,[†,‡] Guosong Hong,[‡,§] Jerry C. Lee,[‡] Jay Patel,[⊥] Bryan Edwards,[⊥] Tatiana S. Zaitseva,[∥] Michael V. Paukshto,[∥] Hongjie Dai,[‡,§] John P. Cooke,[#] Y. Joseph Woo,[‡,⊥] and Ngan F. Huang[*,†,‡,⊥]

[†]Veterans Affairs Palo Alto Health Care System, Palo Alto, California 94304, United States, [‡]Stanford Cardiovascular Institute, Stanford University, Stanford, California 94305, United States, [§]Department of Chemistry, Stanford University, Stanford, California 94305, United States, [⊥]Department of Cardiothoracic Surgery, Stanford University, Stanford, California 94305, United States, [∥]Fibralign Corporation, Union City, California 94587, United States, and [#]Department of Cardiovascular Sciences, Houston Methodist Research Institute, Houston, Texas 77030, United States

ABSTRACT The objective of this study was to enhance the angiogenic capacity of endothelial cells (ECs) using nanoscale signaling cues from aligned nanofibrillar scaffolds in the setting of tissue ischemia. Thread-like nanofibrillar scaffolds with porous structure were fabricated from aligned-braided membranes generated under shear from liquid crystal collagen solution. Human ECs showed greater outgrowth from aligned scaffolds than from nonpatterned scaffolds. Integrin α1 was in part responsible for the enhanced cellular outgrowth on aligned nanofibrillar scaffolds, as the effect was abrogated by integrin α1 inhibition. To test the efficacy of EC-seeded aligned nanofibrillar scaffolds in improving neovascularization *in vivo*, the ischemic limbs of mice were treated with EC-seeded aligned nanofibrillar scaffold; EC-seeded nonpatterned scaffold; ECs in saline; aligned nanofibrillar scaffold alone; or no treatment. After 14 days, laser Doppler blood spectroscopy demonstrated significant improvement in blood perfusion recovery when treated with EC-seeded aligned nanofibrillar scaffolds, in comparison to ECs in saline or no treatment. In ischemic hindlimbs treated with scaffolds seeded with human ECs derived from induced pluripotent stem cells (iPSC-ECs), single-walled carbon nanotube (SWNT) fluorophores were systemically delivered to quantify microvascular density after 28 days. Near infrared-II (NIR-II, 1000−1700 nm) imaging of SWNT fluorophores demonstrated that iPSC-EC-seeded aligned scaffolds group showed significantly higher microvascular density than the saline or cells groups. These data suggest that treatment with EC-seeded aligned nanofibrillar scaffolds improved blood perfusion and arteriogenesis, when compared to treatment with cells alone or scaffold alone, and have important implications in the design of therapeutic cell delivery strategies.

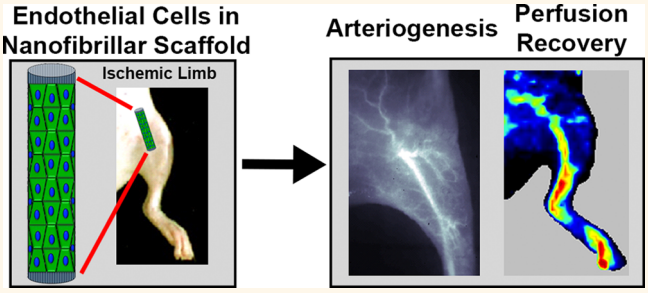

KEYWORDS: nanofibrillar · peripheral arterial disease · induced pluripotent stem cell · angiogenesis · carbon nanotube · ischemia

It is generally agreed that the extracellular matrix (ECM) milieu provides not only structural integrity, but also biophysical and chemical signaling cues to direct cell behavior and function. In native tissues, the ECM secreted by vascular cells forms nano- to microscale fibrillar networks.[1] Bioengineered scaffolds have tremendous potential to advance the fields of tissue engineering and regenerative medicine.[2,3] To elucidate the role of bioengineered scaffolds in modulating cell behavior, a number of properties have been examined, including rigidity, ligand density, porosity, and spatial patterning.[4−9] We and others have previously demonstrated that human microvascular endothelial cells (ECs) respond to parallel-aligned (anisotropic) nanopatterned scaffolds by morphologically reorganizing the cytoskeleton along the direction of the nanofibrils.[10−12] Besides inducing changes at the morphological level, aligned nanofibrillar scaffolds also modulated EC function by enhancing cell survival and by inhibiting inflammation.[13,14] In agreement with our findings, other studies demonstrated a role of nanofibrillar cues in regulating cell function, stem cell differentiation, cellular reprogramming, and tissue morphogenesis.[15−17]

A number of techniques have been developed to engineer nanoscale ECMs,

* Address correspondence to ngantina@stanford.edu.

Received for review January 25, 2015 and accepted June 10, 2015.

Published online June 10, 2015
10.1021/acsnano.5b00545

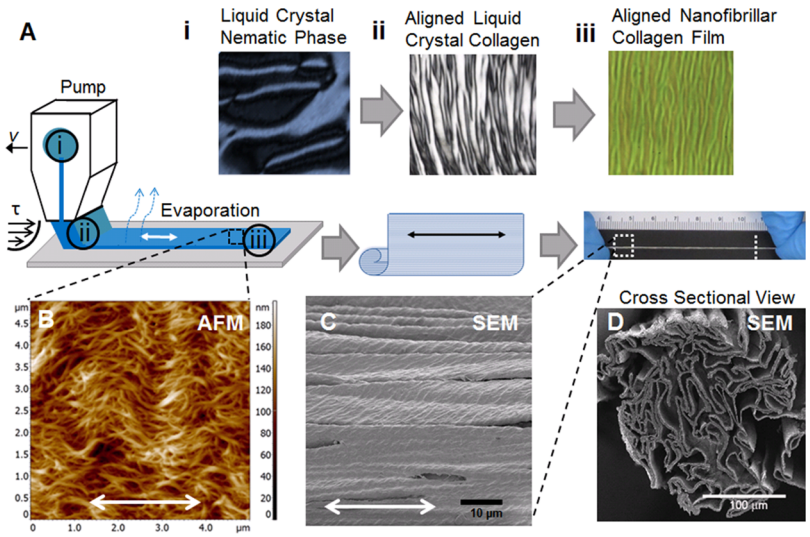

Figure 1. Generation and characterization of aligned collagen scaffold. (A) Schematic of fabricating aligned collagen scaffold in which collagen liquid crystal in the nematic phase (i) is sheared onto glass to create aligned liquid crystal collagen (ii) and then allowed to evaporate, forming an aligned nanofibrillar collagen film (iii). The aligned collagen film then self-assembles into a thread-like scaffold. (B) AFM shows aligned, crimped nanofibrillar scaffold structure. SEM shows the crimped microscale structure along the surface (C) and porous structure by cross-sectional view (D). Scale bars: 10 μm (C), 100 μm (D). Double arrows denote orientation of nanofibrils.

including electrospinning, soft lithography, peptide synthesis, and electron beam lithography.[17−24] We developed a shear-mediated technique to create aligned-braided collagen nanofibrillar scaffolds.[25,26] The advantages of this approach over existing technologies are that it is reproducible and allows the self-assembly of collagen into the structures mimicking collagen native organization. This method takes advantage of monomeric collagen as a lyotropic liquid crystal that undergoes fibrillogenesis selectively along the direction of shear.[25,26] By altering the collagen concentration, ionic strength, and the shear rate, the nanofibril diameter and pattern can be modulated. Parallel-aligned nanofibrillar sheets can be further organized into thread-like porous scaffolds as we demonstrated previously.[14] Unlike injectable hydrogels, these thread-like nanofibrillar scaffolds provide mechanical strength, can be surgically sutured, and can be fabricated at clinically relevant length scales.

In this study, we developed aligned thread-like nanofibrillar collagen scaffolds for treatment of peripheral arterial disease (PAD), which affects over 8 million patients in the US[27] and is characterized by tissue ischemia of the distal limbs due to atherosclerotic lesions that obstruct blood flow. Approaches to enhance angiogenesis and arteriogenesis so as to improve blood flow are promising, but therapeutic cell delivery alone has had only moderate benefit in restoring blood perfusion in clinical trials.[28] We hypothesized that nanofibrillar scaffolds provide signaling cues to enhance the therapeutic potential of ECs. Using both primary ECs as well as ECs derived from human pluripotent stem cells (iPSC-ECs), we show for the first time that aligned nanofibrillar scaffolds enhance the regenerative capacity of transplanted endothelial cells to restore blood perfusion in the ischemic limb and promote arteriogenesis, in part by activation of the transmembrane adhesion molecule, integrin α1 subunit.

RESULTS

Generation of EC-Seeded Aligned Nanofibrillar Scaffold. We fabricated nanofibrillar membranes having helical-like fibrils deposited on plastic substrates. The production process is schematically represented in Figure 1A, in which polarized microscopy images demonstrate the specific features of each step. The starting material is a liquid crystal collagen in nematic phase that shows a typical domain size of 100 μm (Figure 1Ai). The same material under the shear reveals a typical banding period of 10 μm (Figure 1Aii). After evaporation, the resulting aligned nanofibrillar collagen membrane demonstrates a typical crimp periodicity of 3 μm (Figure 1Aiii). AFM analysis of the nanofibrillar collagen membrane on plastic show a nematic structure with highly aligned collagen fibrils with diameter ~30 nm in diameter and an additional translational order formed by the peaks of helices of the helical-like fibrils ("crimp") (Figure 1B). The crimps are perpendicular to the direction of fibril alignment, and collectively, they form the crimp pattern.[26,29] The crimped configurations of collagen fibrils are typical for collagen-based fibrous tissue when external load is reduced, and mimic the woven spiral structure of collagen bundles in relaxed blood vessels.[30] The crimped aligned pattern revealed by AFM was confirmed by corresponding SEM images (Figure 1C). The cross-sectional view revealed that the scaffold was porous and measured approximately

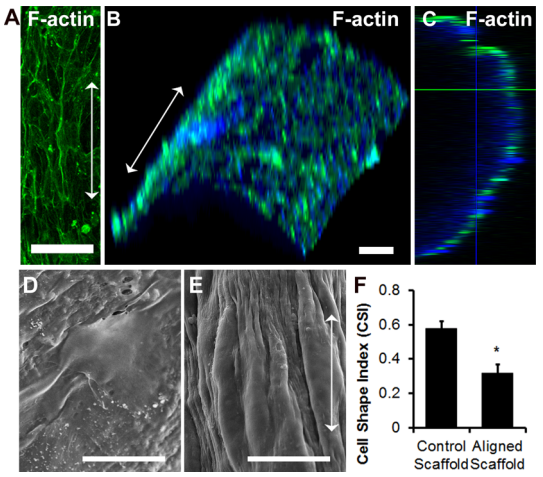

Figure 2. Endothelial morphology on aligned collagen scaffolds. (A) Confocal microscopy images of F-actin fluorescent staining on primary human ECs cultured on aligned nanofibrillar scaffolds. (B) Three-dimensionally reconstructed images showing F-actin staining (green) and Hoechst 33342 total nuclei (blue) surrounding scaffold. (C) Orthogonal view of F-actin staining. SEM of primary human ECs cultured on control (D) scaffold or aligned nanofibrillar (E) scaffolds. (F) Quantification of CSI between cells seeded on control or aligned nanofibrillar scaffolds. Arrow denotes direction of collagen nanofibrils. Scale bar: 100 μm (A,B), 20 μm (D,E).

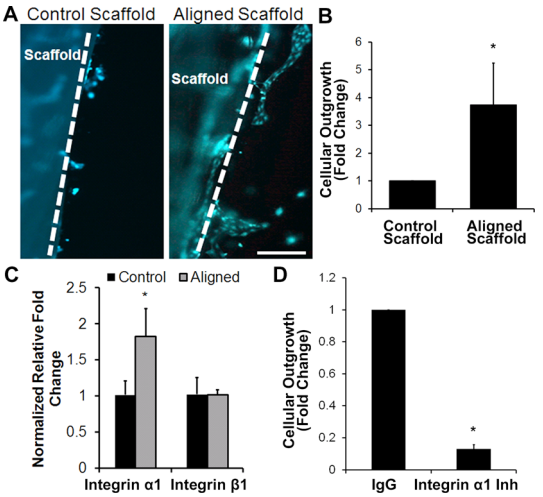

Figure 3. Endothelial outgrowth from aligned nanofibrillar scaffolds. Human ECs seeded on fibronectin-precoated control or aligned scaffold were encapsulated into a 3D hydrogel for tracking cellular outgrowth. (A) Fluorescently labeled ECs are shown migrating from scaffold into the surrounding hydrogel after 3 days. Dotted line denotes border of scaffold. (B) Quantification of cellular outgrowth from control or aligned scaffold after 3 days (n = 3, *P < 0.01). (C) qPCR analysis of integrin subunit gene expression (n = 3, *P < 0.05). (D) Cellular outgrowth from aligned nanofibrillar scaffolds in the presence of integrin α1 inhibition antibody or IgG control (n = 3, *P < 0.001). Scale bar: 200 μm.

300 μm in diameter (Figure 1D). The scaffolds were degradable by collagenase (Figure S1).

Primary human ECs seeded on the aligned nanofibrillar scaffold were elongated and polarized along the direction of nanofibrils, based on F-actin fluorescence staining and SEM (Figure 2A,E), which was in stark contrast to the less elongated morphology of the ECs cultured on the control (nonpatterned) collagen scaffold (Figure 2D). The cells on the aligned nanofibrillar scaffolds surrounded the scaffold, as shown by three-dimensional reconstruction and orthogonal views of the F-actin staining (Figure 2 B,C). Quantification of cell shape index (CSI) as a measure of elongation demonstrated that ECs on aligned nanofibrillar scaffolds were significantly more elongated than cells on the control substrate (Figure 2F, $p < 0.01$).

Aligned Nanofibrillar Scaffold Induces EC Outgrowth through Integrin α1 Activity. To test the ability of aligned nanofibrillar scaffolds to enhance endothelial migration *in vitro*, the fibronectin precoated scaffolds seeded with ECs were embedded into a 3D hydrogel for quantification of cellular outgrowth based on calcein-AM fluorescent dye (Figure 3A) and Hoechst 33342 nuclear stain. After 3 days, the number of ECs that migrated from the nanofibrillar scaffold to the surrounding hydrogel was 3.8 $\pm$ 1.5 times higher in the aligned nanofibrillar scaffold group than in the control group ($p < 0.01$), suggesting that the aligned nanofibrillar scaffold modulated EC activity by inducing significantly greater cellular outgrowth (Figure 3B).

We next sought to elucidate the potential mechanisms of aligned nanofibril-mediated endothelial migration. Given the importance of integrin expression and binding as an important mechanism by which nanotopography modulates cellular effects,[31] we reasoned that collagen-binding integrin $\alpha1\beta1$ may be involved. Quantitative PCR analysis of integrins $\alpha1$ and $\beta1$ demonstrated that ECs cultured on the aligned nanofibrillar substrate had a 1.8 $\pm$ 0.4 times higher expression of integrin $\alpha1$, when compared to control collagen substrate ($p < 0.05$), whereas integrin $\beta1$ expression was not significantly different between the two groups (Figure 3C).

To verify the role of the integrin $\alpha1$ subunit in selectively mediating EC migration on nanopatterned scaffolds, we performed a pharmacological loss-of-function assay using an integrin $\alpha1$ neutralization antibody that was embedded within the surrounding hydrogel. Inactivation of integrin $\alpha1$ reduced EC outgrowth from the aligned nanofibrillar scaffold to 0.13 $\pm$ 0.03 times the value for the isotype-matched negative control group ($p < 0.001$), suggesting that integrin $\alpha1$ is an important mediator of EC outgrowth from aligned nanofibrillar scaffolds (Figure 3D). Fibronectin precoating did not appear to influence the ability of the cells to respond to collagen binding motifs, as cell-seeded scaffolds without fibronectin precoating similarly retained cell attachment capability (Figure S2A) and showed significant reduction in EC outgrowth from aligned nanofibrillar scaffolds in the presence of integrin $\alpha1$ inhibition (0.36 $\pm$ 0.20), relative to isotype-matched negative control group ($p < 0.001$) (Figure S2B).

Aligned Nanofibrillar Scaffolds Seeded with ECs Improve Blood Perfusion in the Ischemic Hindlimb. To verify these

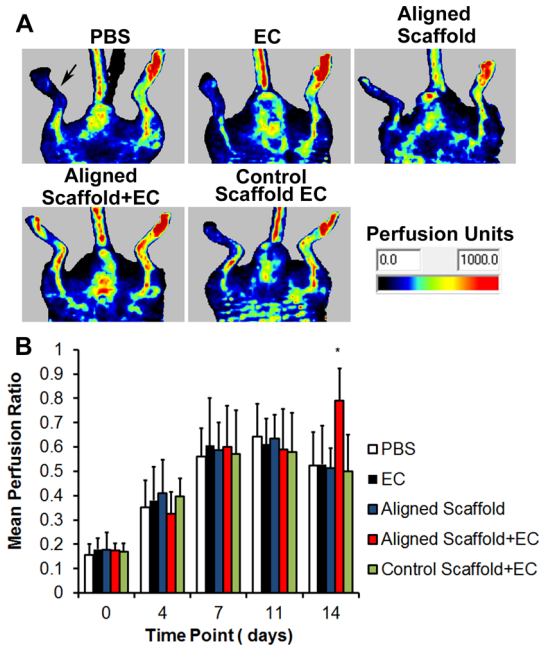

Figure 4. EC-seeded aligned scaffolds enhance limb perfusion after induction of hindlimb ischemia. (A) Representative laser Doppler images showing recovery of perfusion in the ischemic limb (denoted by arrow) after 14 days. (B) Quantification of mean perfusion ratio (ischemic/unoperated limb). *$P < 0.05$, compared to PBS control group ($n \geq 8$).

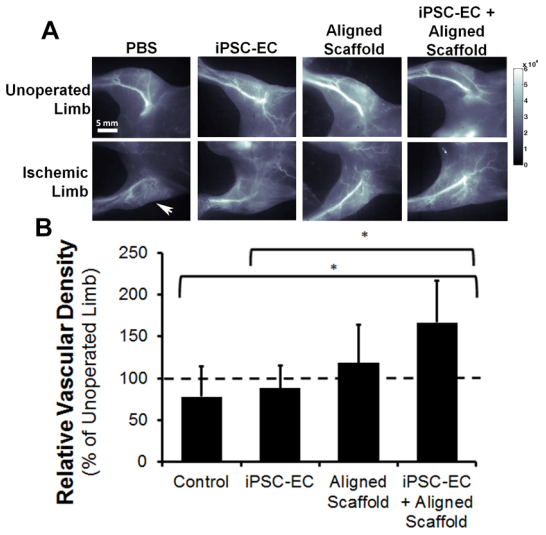

Figure 5. Near infrared-II (NIR-II)-based fluorescence imaging of the hind limb vasculature at 28 days after implantation of aligned scaffold with human iPSC-ECs. (A) Representative images of each group for the ischemic and unoperated limb. (B) Quantification of relative vascular density between treatment groups. Dotted lined denotes vascular density of unoperated limb (*$P < 0.05$, $n \geq 3$).

in vitro results, we next determined whether the aligned scaffolds, in combination with cultured primary ECs, would induce therapeutic enhancement in blood perfusion recovery in a murine model of PAD, which is characterized by limb ischemia upon excision of the femoral artery. At 14 days after treatment, only the animals treated with aligned scaffolds seeded with ECs showed significant blood perfusion recovery when compared to the saline control group ($p < 0.05$, Figure 4A,B). In stark contrast, the animals treated with the control scaffold with ECs, ECs alone, or aligned scaffold alone were not significantly different in mean perfusion ratio, relative to the saline control group (Figure 4B). To understand the mechanism by which the EC-seeded aligned nanofibrillar scaffolds induce angiogenesis, histological analysis of transverse tissue sections after 14 days was performed. Hematoxylin and eosin (H&E)-stained sections showed remnants of the aligned nanofibrillar scaffold (Figure S3A,C), suggesting partial degradation of the scaffold over the course of 2 weeks. Vascular regeneration in the immediate vicinity of the scaffold was evident, based on immunofluorescence staining of murine CD31 for neovessels (Figure S3B,D). These results suggested that the aligned nanofibrillar scaffolds enhance angiogenesis *in vivo* by inducing local neovasculature formation along and around the scaffold.

Aligned Nanofibrillar Scaffolds Seeded with iPSC-ECs Induce Arteriogenesis in the Ischemic Hindlimb. To substantiate these data using therapeutic cells, we generated, purified, and expanded human iPSC-ECs. These cells have been comprehensively characterized in phenotype, transcriptome, and function previously.[32,33] The iPSC-ECs express known endothelial phenotypic markers including von Willebrand factor and CD31 (Figure S4). Similar *in vivo* studies were performed using scaffolds seeded with iPSC-ECs, as a potential infinite source of autologous therapeutic cells. To visualize as well as quantify the formation of new microvasculature noninvasively, we utilized near-infrared in the second window (NIR-II, 1000−1700 nm emission wavelength) imaging of single walled carbon nanotubes (SWNTs) as a fluorescent blood contrast agent, which we previously demonstrated to correlate with histological analysis of neovessel density.[34] Given the limit of detection of ~100 μm vessel diameters using NIR-II-based imaging, the vessels that were detected represented arterioles. As shown in Figure 5A,B, the aligned scaffold seeded with iPSC-ECs demonstrated statistically higher relative vascular density, in comparison to the saline treatment group as well as the iPSC-ECs treatment group ($p < 0.05$, Figure 5B). Quantification of the relative distribution of vessel sizes suggested that the significant increase in arteriogenesis in the aligned scaffold with iPSC-ECs group was attributed to vessels that ranged 151−200 μm in diameter (Figure S5). Immunofluorescence staining of transverse tissue sections confirmed the presence of murine-derived CD31-expressing vessels (Figure S6) in animals treated with the aligned scaffold containing iPSC-ECs. The vessels with visible lumens and having diameters >10 μm (denoted by arrow) were consistent in size with arterioles (Figure S6A), whereas vessels

with flattened lumens <10 μm in diameter were more consistent with capillaries (Figure S6B).[35] Together, these data support our finding that treatment of the ischemic limb with therapeutic endothelial cells cultured on aligned nanofibrillar scaffolds augments arteriogenesis.

DISCUSSION

The salient findings of this work are that (1) EC-seeded aligned nanofibrillar scaffolds promote greater endothelial outgrowth *in vitro* than nonpatterned scaffolds, in part by integrin α1 activation (Figure 3); and (2) EC-seeded aligned nanofibrillar scaffolds enhance blood perfusion and arteriogenesis in the murine ischemic hindlimb, compared to cell delivery or scaffold delivery alone (Figures 4 and 5).

Our results suggest that the therapeutic benefits of cell delivery were augmented when the cells were transplanted while adherent to aligned nanofibrillar scaffolds. Mediating this process was integrin α1, which is abundant in microvascular ECs and is known to be upregulated during angiogenesis.[36] Its activity was necessary for EC outgrowth, since inactivation of integrin α1 abrogated EC outgrowth from the aligned nanofibrillar scaffold *in vitro*. Moreover, integrin activation is also an important mechanism by which cells sense nanotopography. Arnold *et al.* employed nanoscale patterned Au dots with various spacing to probe cell attachment and demonstrated differential integrin activation with different spacing.[31] This study supports a larger body of literature suggesting that integrin interactions with nanopatterned substrates induce morphological as well as biochemical cellular responses.[7]

Besides integrin activation, another mechanism by which aligned nanofibrillar scaffolds promote vascular regeneration is by enabling the transplanted ECs to survive and thereby confer a therapeutic benefit. We previously demonstrated that the aligned nanofibrillar scaffolds sustained iPSC-EC survival for up to 28 days after implantation, whereas cells delivered in saline were no longer detectable by day 4.[14] Notably, in order for iPSC-ECs in saline to enhance blood perfusion after 14 days, we previously showed that an increase in cell number by 2 orders of magnitude (from 4×10^3 to 5×10^5) was required to compensate for the sharp decline in cell viability in the ischemic hindlimb.[33] Therefore, it is likely that aligned nanofibrillar scaffolds promote cell survival as a way to confer regenerative capacity, even at low numbers of transplanted cells.

Compared to conventional cell delivery method in saline, the treatment approach of cell delivery on a supporting scaffold has the advantage of engaging cell adhesion and integrin binding during the process of cell transplantation, as well as localizing cell delivery to the intended delivery site. This study underscores the potential of aligned nanofibrillar scaffolds as a delivery system that can effectively induce therapeutic effects of ECs in ischemic tissues. Being thread-like in shape, the cell-seeded scaffolds can be easily applied to the ischemic tissue in a minimally invasive manner using a commercial tunneling device.

Besides aligned nanofibrillar scaffolds, other methods of engineering scaffolds with angiogenic properties have been developed. For example, Moon *et al.* cocultured ECs with stromal progenitor cells at high cell density within a polyethylene glycol (PEG) hydrogel bearing angiogenic growth factors, and delivery of the cell-encapsulated hydrogel enhanced angiogenesis in the murine cornea.[37] Raghaven *et al.* encapsulated ECs in collagen gel within micropatterned channels and demonstrated that the ECs surrounded the gel in channel so as to mimic a cylindrical vessel-like structure.[38] However, the resulting vascular structures were filled with collagen and did not constitute a hollow lumen. Compared with these two works, our approach focuses on the role of aligned nanofibrillar patterning to guide EC elongation and to attract native ECs toward the scaffold to increase arteriogenesis.

NIR-II-based imaging of vascular regeneration using systemically delivered SWNTs was pioneered by us for noninvasive and sensitive imaging of the microvasculature.[34,39,40] We have shown previously that it has similar imaging resolution with microCT (μCT) and correlates with histological analysis for quantifying blood vessel numbers and sizes.[34] Some of the additional advantages of NIR-II imaging over μCT include greater contrast-to-background ratio, minimum interference from the bones and higher sensitivity of detecting microvascular structures. The nanoscale SWNTs with small molecular weight PEGylated surfactant have short retention time, are biocompatible, and exhibit minimum adverse effect when administered *in vivo*. To our knowledge, this is the first application of NIR-II fluorescence imaging of SWNTs for demonstrating induced arteriogenesis by a bioengineered scaffold with iPSC derivative cells.

Although the present study highlights the beneficial effects of EC-seeded aligned nanofibrillar scaffolds for vascular regeneration, further studies are needed to validate long-term benefits. In addition, further chemical analysis will need to be performed to optimize the retention time and mechanical properties of the scaffold to match the rate of native ECM remodeling. Large animal studies will need to be conducted to determine its suitability for clinical use. A limitation of this study is the use of collagen sutures without nanofibrillar patterning as the basis for comparison to the aligned nanofibrillar scaffold. Because of the fabrication method that utilizes shear to orient liquid crystal collagen, randomly oriented scaffolds produced at reduced shear do not possess sufficient mechanical strength to self-assemble into thread-like scaffolds. Other fabrication methods such as electrospinning may produce

scaffolds that enable direct comparison of fibril alignment on endothelial function. In addition, the control scaffold employed in this study is composed primarily of collagen I,[41] but other types of collagen may be present that may influence cell function.

CONCLUSION

Collectively, this study demonstrates that aligned nanofibrillar scaffolds are a potent cell delivery device to enhance the angiogenic effects of ECs in the ischemic hindlimb. In particular, EC-seeded aligned nanofibrillar scaffolds promoted 3D cellular outgrowth *in vitro* by activating integrin α1, and induced blood perfusion recovery in the ischemic limb after 14 days. Furthermore, iPSC-EC-seeded aligned nanofibrillar scaffolds showed enhanced arteriogenesis in the ischemic hindlimb after 28 days based on NIR-II imaging of systemically perfused vessels. Together, these studies demonstrate that dual treatment of adherent ECs on aligned nanofibrillar scaffolds improved blood perfusion and arteriogenesis, when compared to treatment with cells alone or scaffold alone, and have important implications in the development of therapeutic cell delivery approaches.

MATERIALS AND METHODS

Fabrication of Aligned Nanofibrillar Scaffolds. The aligned nanofibrillar scaffolds were fabricated based on a shear-based fibrillogenesis technique that is suitable for lyotropic liquid crystal materials[42,43] as described previously.[14] In brief, purified monomeric bovine type I collagen solution (Advanced Biomatrix) was concentrated to reach a liquid crystal state[25,29,44,45] and then sheared onto glass or plastic surface,[46] creating thin membranes with parallel-aligned braided nanofibrillar orientation with 30 nm fibril diameter (Figure 1).[46] To make three-dimensional thread-like scaffolds (~10 × 0.3 × 0.3 mm), the membranes were delaminated into a free-standing membrane that was configured into a multiluminal scaffold using liquid−air surface tension.[26] The scaffolds were then cross-linked by dehydrothermal treatment (DHT) at 110 °C under 50 mTorr vacuum for 48 h. As a control scaffold, we used collagen sutures that did not contain ordered nanofibrillar topography (Ethicon, 3−0 plain gut). The scaffolds were characterized using atomic force microscopy (AFM) and scanning electron microscopy (SEM) using routine methods. The polarized microscopy images of liquid crystal collagen were obtained using Leitz Ergolux microscope in transmission mode between crossed polarizers. Prior to cell seeding, the scaffolds were sterilized in 70% ethanol. Where indicated, scaffolds were coated with fibronectin (0.005%) prior to cell seeding.

Scaffold Degradation. Collagen scaffold degradation in collagenase was assayed by measuring soluble protein using ninhydrin reactivity.[47] Briefly, aligned collagen scaffold pieces were incubated at 37 °C in 0.1 M Tris, 0.25 M $CaCl_2$ solution (pH 7.4) containing 125 U/mL bacterial collagenase (Clostridium histolyticum, Calbiochem) for up to 24 h. After incubation, the samples were centrifuged at 15000*g*, and the supernatant was then reacted with 2% ninhydrin reagent (Sigma) in boiling water for 10 min. The optical density was measured at 570 nm in a spectrophotometer (SpectraMAX, Molecular Devices). The relative optical density was calculated by subtracting the value of the background (collagenase only control) from the acquired optical density. The enzymatic degradation of each scaffold type was assayed in replicates of $n = 6$.

Cell Seeding on Nanofibrillar Scaffolds. The primary human dermal microvascular endothelial cells (ECs, Lonza, passage 3−12) and human induced pluripotent stem cell-derived-ECs (iPSC-ECs, passage 8−12)[48] were maintained in EGM2-MV (Lonza) media. The cells were dissociated at a density of 1×10^6/mL and seeded onto scaffolds with or without fibronectin precoating, followed by intermittent shaking for 6 h, resulting in 4×10^3 adherent cells per scaffold. After cell attachment, scaffolds were transferred to ultralow adhesion dishes (Corning). Cell viability was confirmed by the uptake of calcein-AM fluorescence vital dye (Life Technologies).

EC Outgrowth from Nanofibrillar Scaffolds. Cellular outgrowth was assessed in a 3D migration assay using scaffolds with or without fibronectin precoating. One day after EC seeding, the control or aligned nanofibrillar scaffolds were encapsulated within a three-dimensional collagen I hydrogel (1 mg/mL) containing 10% fetal bovine serum and EGM2-MV. After 3 days, the scaffolds were stained with calcein-AM vital dye and then fixed in 4% paraformaldehyde. Cell nuclei were visualized by Hoechst 33342, and 3 fluorescent images were captured for each sample. Cellular outgrowth from the scaffolds was quantified as the total number of cell nuclei that branched from the scaffold into the hydrogel ($n = 3$).

To assess the role of integrin α1 in mediating 3D cell migration on aligned nanofibrillar scaffolds, inhibition studies were performed in which neutralization antibodies directed against mouse antihuman integrin α1 (Millipore, MAB1973Z) or isotype-matched mouse IgG negative control (Millipore, CBL600) were embedded into the collagen hydrogel at 10 μg/mL. Cellular outgrowth after 3 days was quantified as described above ($n = 3$). Aligned nanofibrillar scaffolds with or without fibronectin precoating were assessed to determine whether fibronectin affects integrin α1-mediated endothelial outgrowth ($n = 3$).

Endothelial Cell Morphological Analysis. Elongation of primary ECs on scaffolds was quantified by the cell shape index (CSI) = [(4π × area)/(perimeter^2)], in which CSI = 1.0 indicates a perfect circular cell, whereas CSI = 0.0 represents a line. Primary ECs seeded on either control or aligned nanofibrillar scaffolds were processed routinely and then imaged by SEM for cell morphology. Using ImageJ software (version 1.48), the borders of individual cells on each sample were outlined for measurement of cell area and perimeter, which was used to calculate the CSI ($n \geq 2$). In addition, *in vitro* samples were fluorescently stained for F-actin cytoskeletal assembly using Alexfluor-488-conjugated phalloidin (A12379, Life Technologies) as described previously.[14] Confocal microscopy imaging (Zeiss LSM710) and three-dimensional reconstruction was performed.

Gene Expression Analysis. ECs were cultured on aligned nanofibrillar collagen membranes attached to the glass support without fibronectin precoating. Dishes coated with monomeric collagen I (rat-tail, BD Biosciences, 0.4 mg/mL) served as a control substrate. After 6 days, cells were lysed for RNA extraction using the RNEasy Kit (Qiagen) with modifications,[49] followed by first strand DNA synthesis using Superscript II reverse transcriptase (Life Technologies). Quantitative real-time PCR was performed on a 7300 Real-Time PCR system (Life Technologies). Taqman primers consisted of integrins α1 (Hs00235006_m1) and β1 (Hs01127543_m1) and housekeeping gene GAPDH (HS99999905_m1). Relative fold change in gene expression was calculated using the ΔΔCt method and normalized to GAPDH housekeeping gene expression ($n = 3$).

Hindlimb Ischemia and Scaffold Implantation. The efficacy of the aligned nanofibrillar scaffold to support angiogenesis and arteriogenesis was examined in the murine hindlimb ischemia model, which mimics PAD. Aligned or control scaffolds (1 cm long) were precoated with fibronectin before seeding with primary ECs. Unilateral hindlimb ischemia was induced in male NOD SCID (13−16 weeks old) by excision of the femoral artery as previously described.[50] The animals were randomized to receive one of the following treatments at the excision site in the femoral artery bed: (1) aligned nanofibrillar scaffold seeded

with ECs; (2) control scaffold seeded with ECs; (3) aligned nanofibrillar scaffold without cells; (4) 4×10^3 ECs in 30 μL of PBS; or (5) 30 μL of PBS ($n \geq 8$). The scaffolds were implanted and sutured to the remaining free ends of the femoral artery left after its excision (Figure S7). Cells or saline treatment was injected into the ischemic adductor muscle. Recovery of blood perfusion was assessed at regular time intervals over 14 days using laser Doppler spectroscopy, for which the data are expressed as the mean perfusion ratio = (perfusion in ischemic limb)/(perfusion in unoperated limb).

To assess the application of human iPSC-ECs as a therapeutic cell source, hindlimb ischemia studies were performed in which the mice were randomized into the following groups: (1) aligned nanofibrillar scaffold seeded with iPSC-ECs; (2) aligned nanofibrillar scaffold without cells; (3) 4×10^3 iPSC-ECs in 30 μL of PBS; or (4) 30 μL of PBS ($n \geq 3$). Noninvasive imaging of arteriogenesis in the hindlimbs was assessed after 28 days using NIR-II as described below. All animal experiments were performed with approval by the Administrative Panel on Laboratory Animal Care in Stanford University.

Intravital NIR-II Imaging of Arteriogenesis. NIR-II fluorescence imaging of hindlimb vasculature in live mice was performed with a homemade NIR-II imaging system as described in our previous publications.[34,39] In brief, each animal was injected with a 200 μL solution of SWNT NIR-II fluorophores coated with DSPE-mPEG (5 kDa) (1,2-distearoyl-*sn*-glycero-3-phosphoethanolamine-*N*-[methoxy(polyethylene glycol, 5000)], Laysan Bio) at a concentration of 0.10 mg/mL for SWNTs through the tail vein. At approximately 10 min post injection, each animal was placed on the imaging stage in the supine position, and the hindlimb area was positioned within the field of view (25 mm $\times$ 20 mm). The field of view was illuminated with a fiber-coupled 808 nm diode laser (RMPC lasers) through a 4.5 mm collimator (Thorlabs) to reach an in-plane power density of 140 mW/cm^2. An 850 nm short-pass filter and a 1000 nm short-pass filter (Thorlabs) were used as excitation filters to remove the long-wavelength light from the laser. The fluorescence emission from the SWNT fluorophores circulating in the hindlimb vasculature was collected using a 200 mm achromat and a 75 mm achromat (Thorlabs, both with antireflective coating in the NIR-II window), and filtered through a 900 nm long-pass filter and an 1100 nm long-pass filter (Thorlabs) to remove the laser light. The filtered fluorescence in the range of 1100−1700 nm was focused onto a liquid-nitrogen cooled, 2D indium−gallium-arsenide (InGaAs) detector array (Princeton Instruments 2D OMA-V), which captured static fluorescence images of the mouse hindlimb with an exposure time of 100−300 ms, depending on the brightness and the actual injection dose of the SWNTs.

After NIR-II fluorescence images were acquired with the 2D InGaAs camera, a line profile peak counting method, which was described in detail in our previous publication,[34] was used to analyze the relative microvascular density of the ischemic hindlimb in comparison to the control hindlimb. Briefly, two horizontal lines were drawn medially and laterally to the femoral vessels and two vertical lines were drawn perpendicularly to the previous two lines near the proximal and distal ends of the femoral vessels (Figure S8). The line profile of NIR-II fluorescence intensity along each line was extracted and plotted in the ImageJ software, where peaks in the line profile were assigned as blood vessels. Since the two vertical lines intersect the same femoral vessels twice, these double counted vessels were subtracted from the total number of vessels. To find the relative microvascular density of the ischemic hindlimb, the total number of vessels found in the ischemic hindlimb was divided by that found in the control hindlimb.

Histology and Immunofluorescence Staining. At specified time points, the mice were euthanized, and the adductor muscles were excised together with the scaffolds for cryosectioning. Tissue sections were stained with hematoxylin and eosin (H&E) for histological analysis. Murine microvasculature adjacent to the scaffold was visualized using rat antimouse CD31 (BD Pharmingen, 550274) antibody, followed by goat antirat Alexfluor-488 (A11006, Life Technologies) or Alexafluor-594 (A11032, Life Technologies) secondary antibodies, according to our previous publications.[33,34] Total nuclei were stained by Hoechst 33342 dye (Life Technologies).

Statistical Analysis. All data are shown as mean $\pm$ standard deviation. Statistical comparisons between 2 groups were quantified by an unpaired *t*-test. For comparisons of 3 or more groups, analysis of variance (ANOVA) with Holm's adjustment for multiple comparisons was used. Statistical significance was accepted at $p < 0.05$.

Conflict of Interest: The authors declare the following competing financial interest(s): Fibralign Corporation produces the aligned nanofibrillar collagen scaffolds we have used in this study. M.V.P is CTO and T.S.Z. is a leading researcher of Fibralign Corporation. All remaining authors declare no competing financial interests.

Acknowledgment. This study was supported in part by grants from the US National Institutes of Health (HL098688, and EB0202351 to N.F.H.; and 1T32HL098049 to K.H.N., the US Army Medical Research and Materiel Command (W81XWH-12-C-0111 to M.V.P.), the National Science Foundation (1249008 to M.V.P.), the Stanford Chemistry Engineering & Medicine for Human Health (to N.F.H.), and the Stanford Cardiovascular Institute (to N.F.H.). We thank Janet Okogbaa and Arshi Jha for technical assistance, Lydia-Marie Joubert for assistance with SEM, and Marie Madeleine Giraud-Guille for her advice on polarized microscope imaging of liquid crystal collagen.

Supporting Information Available: Analysis of scaffold degradation by collagenase; vessel density quantification from NIR-II imaging; immunofluorescence staining of purified human iPSC-ECs for endothelial phenotypic markers; immunohistological analysis of angiogenesis surrounding the aligned scaffold at 2 weeks after implantation; NIR-II imaging quantification of vessel size distribution in the ischemic limb between treatment groups after 28 days; immunofluorescence imaging of murine CD31 in animals that received treatment of the aligned nanofibrillar scaffold with iPSC-ECs at 4 weeks after implantation; schematic diagram of scaffold implantation; and integrin inhibition studies on aligned nanofibrillar scaffolds without fibronectin precoating. The Supporting Information is available free of charge on the ACS Publications website at DOI: 10.1021/acsnano.5b00545.

REFERENCES AND NOTES

1. Kim, D. H.; Provenzano, P. P.; Smith, C. L.; Levchenko, A. Matrix Nanotopography as a Regulator of Cell Function. *J. Cell Biol.* **2012**, *197*, 351–360.
2. Huebsch, N.; Mooney, D. J. Inspiration and Application in the Evolution of Biomaterials. *Nature* **2009**, *462*, 426–432.
3. Ratner, B. D.; Bryant, S. J. Biomaterials: Where We Have Been and Where We Are Going. *Annu. Rev. Biomed. Eng.* **2004**, *6*, 41–75.
4. Gilbert, P. M.; Havenstrite, K. L.; Magnusson, K. E.; Sacco, A.; Leonardi, N. A.; Kraft, P.; Nguyen, N. K.; Thrun, S.; Lutolf, M. P.; Blau, H. M. Substrate Elasticity Regulates Skeletal Muscle Stem Cell Self-Renewal in Culture. *Science* **2010**, *329*, 1078–1081.
5. Kshitiz; Hubbi, M. E.; Ahn, E. H.; Downey, J.; Afzal, J.; Kim, D. H.; Rey, S.; Chang, C.; Kundu, A.; Semenza, G. L.; Abraham, R. M.; *et al.* Matrix Rigidity Controls Endothelial Differentiation and Morphogenesis of Cardiac Precursors. *Sci. Signaling* **2012**, *5*, ra41.
6. He, L.; Zhang, Y.; Zeng, C.; Ngiam, M.; Liao, S.; Quan, D.; Zeng, Y.; Lu, J.; Ramakrishna, S. Manufacture of Plga Multiple-Channel Conduits with Precise Hierarchical Pore Architectures and *in Vitro/Vivo* Evaluation for Spinal Cord Injury. *Tissue Eng., Part C* **2009**, *15*, 243–255.
7. Dalby, M. J.; Gadegaard, N.; Oreffo, R. O. Harnessing Nanotopography and Integrin-Matrix Interactions to Influence Stem Cell Fate. *Nat. Mater.* **2014**, *13*, 558–569.
8. Liliensiek, S. J.; Wood, J. A.; Yong, J.; Auerbach, R.; Nealey, P. F.; Murphy, C. J. Modulation of Human Vascular Endothelial Cell Behaviors by Nanotopographic Cues. *Biomaterials* **2010**, *31*, 5418–5426.

9. Straley, K. S.; Heilshorn, S. C. Design and Adsorption of Modular Engineered Proteins to Prepare Customized, Neuron-Compatible Coatings. *Front. Neuroeng.* **2009**, *2*, 9.
10. Lai, E. S.; Huang, N. F.; Cooke, J. P.; Fuller, G. G. Aligned Nanofibrillar Collagen Regulates Endothelial Organization and Migration. *Regener. Med.* **2012**, *7*, 649–661.
11. Wu, H.; Fan, J.; Chu, C. C.; Wu, J. Electrospinning of Small Diameter 3-D Nanofibrous Tubular Scaffolds with Controllable Nanofiber Orientations for Vascular Grafts. *J. Mater. Sci.: Mater. Med.* **2010**, *21*, 3207–3215.
12. Ma, Z.; He, W.; Yong, T.; Ramakrishna, S. Grafting of Gelatin on Electrospun Poly(Caprolactone) Nanofibers to Improve Endothelial Cell Spreading and Proliferation and to Control Cell Orientation. *Tissue Eng.* **2005**, *11*, 1149–1158.
13. Huang, N. F.; Lai, E. S.; Ribeiro, A. J.; Pan, S.; Pruitt, B. L.; Fuller, G. G.; Cooke, J. P. Spatial Patterning of Endothelium Modulates Cell Morphology, Adhesiveness and Transcriptional Signature. *Biomaterials* **2013**, *34*, 2928–2937.
14. Huang, N. F.; Okogbaa, J.; Lee, J. C.; Jha, A.; Zaitseva, T.; Paukshto, M.; Sun, J.; Fuller, G. G.; Cooke, J. P. The Modulation of Endothelial Cell Morphology, Function, and Survival Using Anisotropic Nanofibrillar Collagen Scaffolds. *Biomaterials* **2013**, *34*, 4038–4047.
15. Yang, J.; McNamara, L. E.; Gadegaard, N.; Alakpa, E. V.; Burgess, K. V.; Meek, R. M.; Dalby, M. J. Nanotopographical Induction of Osteogenesis through Adhesion, Bone Morphogenic Protein Cosignaling, and Regulation of Micrornas. *ACS Nano* **2014**, *8*, 9941–9953.
16. Downing, T. L.; Soto, J.; Morez, C.; Houssin, T.; Fritz, A.; Yuan, F.; Chu, J.; Patel, S.; Schaffer, D. V.; Li, S. Biophysical Regulation of Epigenetic State and Cell Reprogramming. *Nat. Mater.* **2013**, *12*, 1154–1162.
17. Huang, N. F.; Patel, S.; Thakar, R. G.; Wu, J.; Hsiao, B. S.; Chu, B.; Lee, R. J.; Li, S. Myotube Assembly on Nanofibrous and Micropatterned Polymers. *Nano Lett.* **2006**, *6*, 537–542.
18. He, W.; Yong, T.; Ma, Z. W.; Inai, R.; Teo, W. E.; Ramakrishna, S. Biodegradable Polymer Nanofiber Mesh to Maintain Functions of Endothelial Cells. *Tissue Eng.* **2006**, *12*, 2457–2466.
19. Murugan, R.; Ramakrishna, S. Design Strategies of Tissue Engineering Scaffolds with Controlled Fiber Orientation. *Tissue Eng.* **2007**, *13*, 1845–1866.
20. Li, D.; Wang, Y.; Xia, Y. Electrospinning of Polymeric and Ceramic Nanofibers as Uniaxially Aligned Arrays. *Nano Lett.* **2003**, *3*, 1167–1171.
21. Qin, D.; Xia, Y.; Whitesides, G. M. Soft Lithography for Micro- and Nanoscale Patterning. *Nat. Protoc.* **2010**, *5*, 491–502.
22. Vieu, C.; Carcenac, F.; Pepin, A.; Chen, Y.; Mejias, M.; Lebib, A.; Manin-Ferlazzo, L.; Couraud, L.; Launois, H. Electron Beam Lithography: Resolution Limits and Applications. *Appl. Surf. Sci.* **2000**, *164*, 111–117.
23. Kumar, V. A.; Taylor, N. L.; Shi, S.; Wang, B. K.; Jalan, A. A.; Kang, M. K.; Wickremasinghe, N. C.; Hartgerink, J. D. Highly Angiogenic Peptide Nanofibers. *ACS Nano* **2015**, *9*, 860–868.
24. Davis, M. E.; Hsieh, P. C.; Takahashi, T.; Song, Q.; Zhang, S.; Kamm, R. D.; Grodzinsky, A. J.; Anversa, P.; Lee, R. T. Local Myocardial Insulin-Like Growth Factor 1 (Igf-1) Delivery with Biotinylated Peptide Nanofibers Improves Cell Therapy for Myocardial Infarction. *Proc. Natl. Acad. Sci. U. S. A.* **2006**, *103*, 8155–8160.
25. Paukshto, M.; McMurtry, D.; Bobrov, Y.; Sabelman, E. Oriented Collagen-Based Materials, Films and Methods of Making Same. *World Intellectual Property Organization* 2008, WO/2008/131293.
26. Paukshto, M. V.; McMurtry, D. H.; Martin, G. R.; Zaitseva, T.; Bobrov, Y. A. Biocomposites and Methods of Making the Same. *World Intellectual Property Organization* 2010, WO/2010/019625.
27. Go, A. S.; Mozaffarian, D.; Roger, V. L.; Benjamin, E. J.; Berry, J. D.; Borden, W. B.; Bravata, D. M.; Dai, S.; Ford, E. S.; Fox, C. S.; Franco, S.; *et al.* Heart Disease and Stroke Statistics—2013 Update: A Report from the American Heart Association. *Circulation* **2013**, *127*, e6–e245.
28. Annex, B. H. Therapeutic Angiogenesis for Critical Limb Ischaemia. *Nat. Rev. Cardiol.* **2013**, *10*, 387–396.
29. Muthusubramaniam, L.; Peng, L.; Zaitseva, T.; Paukshto, M.; Martin, G. R.; Desai, T. A. Collagen Fibril Diameter and Alignment Promote the Quiescent Keratocyte Phenotype. *J. Biomed. Mater. Res., Part A* **2012**, *100*, 613–621.
30. Arkill, K. P.; Moger, J.; Winlove, C. P. The Structure and Mechanical Properties of Collecting Lymphatic Vessels: An Investigation Using Multimodal Nonlinear Microscopy. *J. Anat.* **2010**, *216*, 547–555.
31. Arnold, M.; Cavalcanti-Adam, E. A.; Glass, R.; Blummel, J.; Eck, W.; Kantlehner, M.; Kessler, H.; Spatz, J. P. Activation of Integrin Function by Nanopatterned Adhesive Interfaces. *ChemPhysChem* **2004**, *5*, 383–388.
32. White, M. P.; Rufaihah, A. J.; Liu, L.; Ghebremariam, Y. T.; Ivey, K. N.; Cooke, J. P.; Srivastava, D. Limited Gene Expression Variation in Human Embryonic Stem Cell and Induced Pluripotent Stem Cell-Derived Endothelial Cells. *Stem Cells* **2013**, *31*, 92–103.
33. Rufaihah, A. J.; Huang, N. F.; Jame, S.; Lee, J. C.; Nguyen, H. N.; Byers, B.; De, A.; Okogbaa, J.; Rollins, M.; Reijo-Pera, R.; Gambhir, S. S.; *et al.* Endothelial Cells Derived from Human Ipscs Increase Capillary Density and Improve Perfusion in a Mouse Model of Peripheral Arterial Disease. *Arterioscler., Thromb., Vasc. Biol.* **2011**, *31*, e72–e79.
34. Hong, G.; Lee, J. C.; Jha, A.; Diao, S.; Nakayama, K. H.; Hou, L.; Doyle, T. C.; Robinson, J. T.; Antaris, A. L.; Dai, H.; Cooke, J. P.; *et al.* Near-Infrared II Fluorescence for Imaging Hindlimb Vessel Regeneration with Dynamic Tissue Perfusion Measurement. *Circ.: Cardiovasc. Imaging* **2014**, *7*, 517–525.
35. Kellar, R. S.; Landeen, L. K.; Shepherd, B. R.; Naughton, G. K.; Ratcliffe, A.; Williams, S. K. Scaffold-Based Three-Dimensional Human Fibroblast Culture Provides a Structural Matrix That Supports Angiogenesis in Infarcted Heart Tissue. *Circulation* **2001**, *104*, 2063–2068.
36. Defilippi, P.; van Hinsbergh, V.; Bertolotto, A.; Rossino, P.; Silengo, L.; Tarone, G. Differential Distribution and Modulation of Expression of Alpha 1/Beta 1 Integrin on Human Endothelial Cells. *J. Cell Biol.* **1991**, *114*, 855–863.
37. Moon, J. J.; Saik, J. E.; Poche, R. A.; Leslie-Barbick, J. E.; Lee, S. H.; Smith, A. A.; Dickinson, M. E.; West, J. L. Biomimetic Hydrogels with Pro-Angiogenic Properties. *Biomaterials* **2010**, *31*, 3840–3847.
38. Raghavan, S.; Nelson, C. M.; Baranski, J. D.; Lim, E.; Chen, C. S. Geometrically Controlled Endothelial Tubulogenesis in Micropatterned Gels. *Tissue Eng., Part A* **2010**, *16*, 2255–2263.
39. Hong, G.; Lee, J. C.; Robinson, J. T.; Raaz, U.; Xie, L.; Huang, N. F.; Cooke, J. P.; Dai, H. Multifunctional *in Vivo* Vascular Imaging Using Near-Infrared II Fluorescence. *Nat. Med.* **2012**, *18*, 1841–1846.
40. Hong, G.; Diao, S.; J, C.; Antaris, A. L.; Chen, C.; Zhang, B.; Zhao, S.; Atochin, D. N.; Huang, P. L.; Andreasson, K. I.; Kuo, C. J.; *et al.* Through-Skull Fluorescence Imaging of the Brain in a New Near-Infrared Window. *Nat. Photonics* **2014**, *8*, 723–730.
41. Graham, M. F.; Diegelmann, R. F.; Elson, C. O.; Lindblad, W. J.; Gotschalk, N.; Gay, S.; Gay, R. Collagen Content and Types in the Intestinal Strictures of Crohn's Disease. *Gastroenterology* **1988**, *94*, 257–265.
42. Paukshto, M.; Fuller, G.; Michailov, A.; Remizov, S. Optics of Sheared Liquid-Crystal Polarizer Based on Aqueous Dispersion of Dichroic-Dye Nano-Aggregates. *J. Soc. Inf. Disp.* **2005**, *13*, 765–772.
43. Ukai, Y.; Ohyama, T.; Fennell, L.; Kato, Y.; Paukshto, M.; Smith, P.; Yamashita, O.; Nakanishi, S. Current Status and Future Prospect of in-Cell Polarizer Technology. *SID Symp. Dig.* **2004**, *35*, 1170–1173.
44. Kirkwood, J. E.; Fuller, G. G. Liquid Crystalline Collagen: A Self-Assembled Morphology for the Orientation of Mammalian Cells. *Langmuir* **2009**, *25*, 3200–3206.
45. Bobrov, Y.; Fennell, L.; Lazarev, P.; Paukshto, M.; Remizov, S. Manufacturing of a Thin-Film Lcd. *J. Soc. Inf. Disp.* **2002**, *10*, 317–321.

46. McMurtry, D.; Paukshto, M.; Bobrov, Y. A Liquid Film Applicator Assembly and Rectilinear Shearing System Incorporating the Same. *World Intellectual Property Organization* 2008, WO/2008/063631.
47. Starcher, B. A Ninhydrin-Based Assay to Quantitate the Total Protein Content of Tissue Samples. *Anal. Biochem.* **2001**, *292*, 125–129.
48. Huang, N. F.; Dewi, R. E.; Okogbaa, J.; Lee, J. C.; Jalilrufaihah, A.; Heilshorn, S. C.; Cooke, J. P. Chemotaxis of Human Induced Pluripotent Stem Cell-Derived Endothelial Cells. *Am. J. Transl. Res.* **2013**, *5*, 510–520.
49. Yu, J.; Huang, N. F.; Wilson, K. D.; Velotta, J. B.; Huang, M.; Li, Z.; Lee, A.; Robbins, R. C.; Cooke, J. P.; Wu, J. C. Nachrs Mediate Human Embryonic Stem Cell-Derived Endothelial Cells: Proliferation, Apoptosis, and Angiogenesis. *PLoS One* **2009**, *4*, e7040.
50. Niiyama, H.; Huang, N. F.; Rollins, M. D.; Cooke, J. P. Murine Model of Hindlimb Ischemia. *J. Visualized Exp.* **2009**, *23*, 1035.